THE JOURNAL OF PHYSICAL CHEMISTRY B

Article

pubs.acs.org/JPCB

Fractal Self-Assembly of Single-Stranded DNA on Hydrophobic Self-Assembled Monolayers

Chunyan Xing,[†,‡] Haiyan Qiao,[†,‡] Yongjun Li,[†,‡] Xi Ke,[†,‡] Zhe Zhang,[†] Bailin Zhang,*[,†] and Jilin Tang*[,†]

[†]State Key Laboratory of Electroanalytical Chemistry, Changchun Institute of Applied Chemistry, Chinese Academy of Sciences, Changchun 130022, People's Republic of China

[‡]Graduate University of Chinese Academy of Sciences, Beijing 100049, People's Republic of China

ABSTRACT: The self-assembled structures possess superior stability, biocompatibility and mechanical strength, and their study can provide insight into the use of creating novel biomaterials. Atomic force microscopy (AFM) images of single-stranded DNA (ssDNA) nanostructures show that well-ordered organization, high homogeneity, and molecular dimensions fractal-shaped fibers formed on a gold substrate covered with self-assembled monolayers (SAMs) of 1-hexadecanethiol (HDT). The nanoscaled architectures of ssDNA on HDT/Au changed remarkably following the process of diffusion-limited cluster aggregation (DLA) over time. The ssDNA fibers prefer to form on hydrophobic SAMs instead of hydrophilic SAMs, and the ssDNA has to have complementary regions in their sequences. This method might not be used only for the construction of fractal patterns, but also for the design and fabrication of functional DNA-based, self-assembled materials that exhibit self-similarity at multiple length scales.

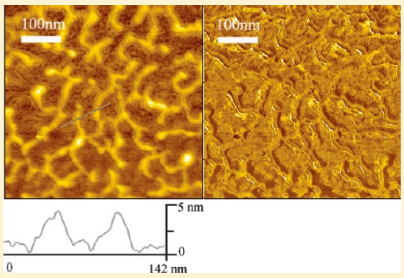

INTRODUCTION

Molecular self-assembly is ubiquitous for the formation of diverse and complex biological structures that can form designed structures rapidly, reversibly, and controllably.[1] Besides its well-ordered organization, high homogeneity, and molecular dimensions, the self-assembled structures possess superior stability, biocompatibility, and mechanical strength.[2] By weak and noncovalent interactions, biomolecules self-assembling to form functional supramolecular structures is of outstanding interest from fundamental as well as applied perspectives.[3−5] In addition, autonomous assembly from components with an apparent lack of order into well-structured complexes can be used to create novel biomaterials, which have been the subject of considerable research due to their outstanding properties.[1,6]

By theoretical models and computer simulations, self-assembly and organization progresses are generally modeled on the basis of architecture, dimensionality, and kinetic regimes-fast, diffusion-limited cluster aggregation (DLA).[7−9] The aggregation progress occurs as the solvent evaporates and the component deposits on the substrate, eventually resulting in a fractal structure. Over a limited range of length scales, many structures have fractal geometry with self-similarity at long and short lengths. The fractal structures formed from biomolecules lie down on the surface at designated positions, thereby preventing mutual superimposition in a disordered arrangement. These structures prelude promising interesting applications, especially toward future nano-optics[10,11] and biotemplating.[12] Therefore, the formation of fractal structures is an interesting topic for more detailed theoretical and technological studies.

The formation of fractal structures from DNA on a solid surface has been seldom reported.[12−15] Long DNA molecule structures can be characterized by AFM. However, short, single-stranded DNA (ssDNA) with several tens of bases on solid surface are invisible by AFM because they were dragged by the AFM tip and move with the AFM tip during the scanning. Here, ssDNA fractal nanostructures were formed on a gold substrate covered with a self-assembled monolayer (SAM) of 1-hexadecanethiol (HDT). Atomic force microscopy (AFM) was applied to monitor the formation of fractal nanostructures of ssDNA at different incubation times with high-resolution imaging. The nanoscaled architectures of ssDNA on HDT/Au changed remarkably following the process of DLA over time. The distinctive fractal behavior is representative for a series of ssDNA molecules having complementary sequences between two individual ssDNA. The construction of ssDNA fractal architectures on hydrophobic self-assembled monolayer are visible by AFM, which has not previously been reported. It provides a simple way to fabricate shape-controllable ssDNA nanowires at designated positions, which avoids superimposition and mutual contact. It opens new possibilities for the design and fabrication of functional DNA-based, self-assembled materials that exhibit self-similarity at multiple length scales.

EXPERIMENTAL SECTION

Chemicals and Reagents. The following single-stranded DNA (ssDNA) probes: 5′- GCC GGC CAC AGC CAA TCA

Received: June 26, 2012
Revised: September 2, 2012
Published: September 6, 2012

dx.doi.org/10.1021/jp306269n | J. Phys. Chem. B 2012, 116, 11594−11599

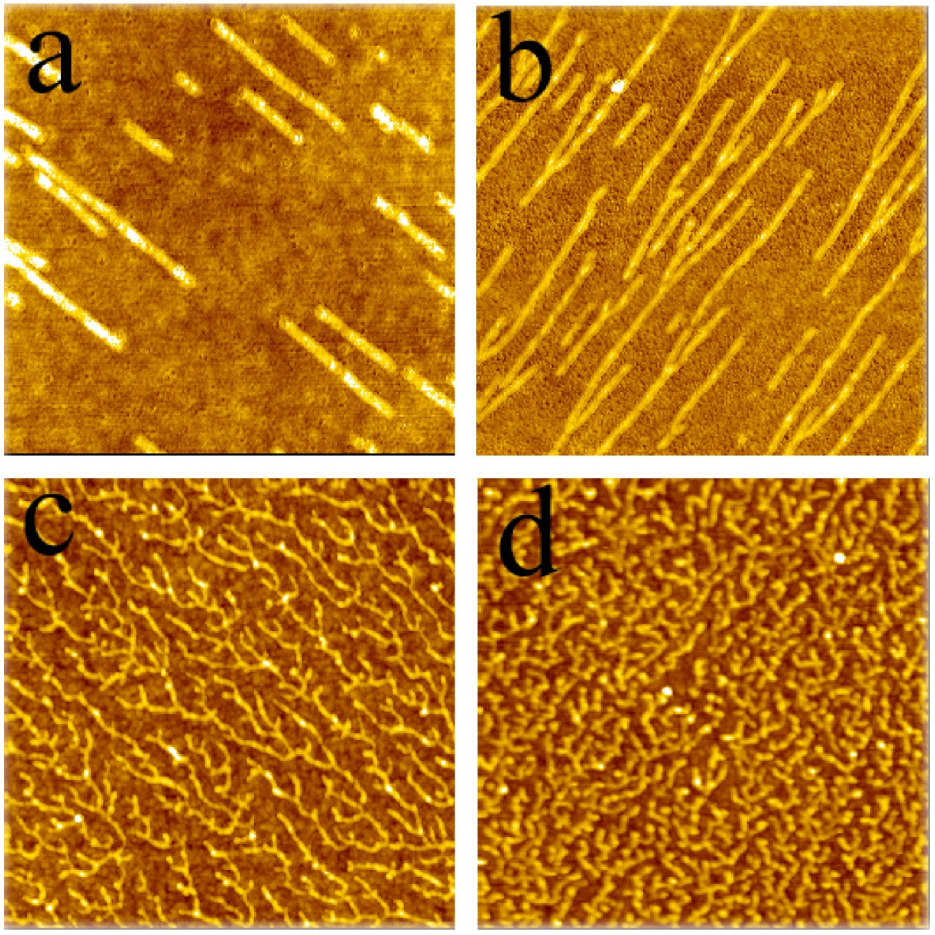

Figure 1. AFM topographic images of ssDNA (probe 1) fibers on HDT/Au incubated in 1 μmol/L ssDNA for various developing times: 5 (a), 10 (b), 14 (c), and 22 h (d). The scanning size is 2.0 × 2.0 μm^2.

GCA GCG CGG ACC CCT CCC CAG GGC GGA GCT GAC GGC C -3′ (probe 1), 5′- AGT CCG TGG TAG GGC AGG TTG GGG TGA CT -3′ (probe 2), 5′- CAG GCT ACG GCA CGT AGA GCA TCA CCA TGA TCC TG -3′ (probe 3), 5′- GGG GCA CGT TTA TCC GTC CCT CCT AGT GGC GTG CCC C -3′ (probe 4), and poly-T_{70} (probe 5) were synthesized by Sangon (Shanghai, China). 1-Hexadecanethiol (HDT), 16-mercaptohexadecanoic acid (MHA), 4-amino-thiophenol (4-ATP), 6-mercapto-1-hexanol (MCH), and 1-dodecanethiol (DDT) were purchased from Aldrich and used without further purification. All aqueous solutions were prepared with Milli-Q water (>18.2 MΩ·cm) from a Milli-Q Plus system (Millipore). A 10 mM Tris-HCl (pH = 7.40, 50 mM NaCl) buffer solution was used.

Preparation of SAMs on Gold Substrate. The gold slides, 50 nm thick gold films deposited on 5 nm chromium precoated on microscope glass slides (8 × 8 × 0.18 mm), were prepared by e-beam evaporation on glass substrates in a vacuum chamber (Denton Vacuum, model DV 502-A) at a background pressure below 2 × 10^{-6} Torr. The glass was preheated to 350 °C before deposition. After evaporation, Au films were annealed at 360 °C under vacuum for 30 min and then cooled to room temperature. The gold slides were immersed in a 1.0 mM HDT, MHA, 4-ATP, MCH, and DDT in ethanol solution at room temperature for at least 24 h, respectively. The gold slides with SAMs of mercaptan were rinsed copiously with ethanol and Milli-Q water before being incubated with ssDNA.

Fractal-Shaped ssDNA Fibers (probe 1) Formation. The SAMs of HDT were incubated with 1 μM/L ssDNA (probe 1) at room temperature for 5, 10, 14, and 22 h, respectively. This resulted in the formation of fractal-shaped ssDNA fibers. For investigating the effect of terminal groups of SAMs on forming fractal-shaped ssDNA fibers, MHA, 4-ATP, MCH, and DDT SAMs were incubated with 1 μM/L ssDNA (probe 1) for 22 h, respectively. For investigating the effects complementary regions in ssDNA have on the forming fractal-shape fibers, the SAM of HDT were incubated with DNA (probe 2), ssDNA (probe 3), ssDNA (probe 4), and ssDNA (probe 5) for 22 h, respectively.

AFM Measurement. After the treatment above, the sample was rinsed copiously with Milli-Q water and then dried in air. All AFM experiments were performed on AFM (SPA-400, SII, Japan) in tapping mode. A tapping mode AFM tip (PPP-SEIHR probe with a spring constant of 8.8 N/m, resonant frequency 117 kHz) was used to observe the ssDNA topography. The AFM images were acquired in air under ambient conditions at a relative humidity of 60%.

■ RESULTS AND DISCUSSION

AFM images of DNA fibers for different incubation time. After the gold slide with SAMs of HDT was incubated in 1 μmol/L ssDNA (probe 1) at room temperature for 5, 10, 14, and 22 h, a

dx.doi.org/10.1021/jp306269n | J. Phys. Chem. B 2012, 116, 11594−11599

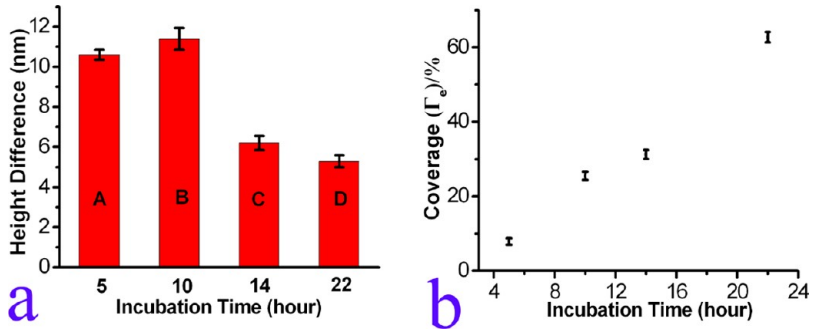

Figure 2. (a) Histograms of the height for ssDNA (probe 1) fibers formed on HDT/Au in 1 μmol/L ssDNA for various developing times: 5 (A), 10 (B), 14 (C), and 22 h (D). (b) Plot of the estimated surface coverage (Γ_e) of ssDNA (probe 1) fibers as a function of developing time in ssDNA.

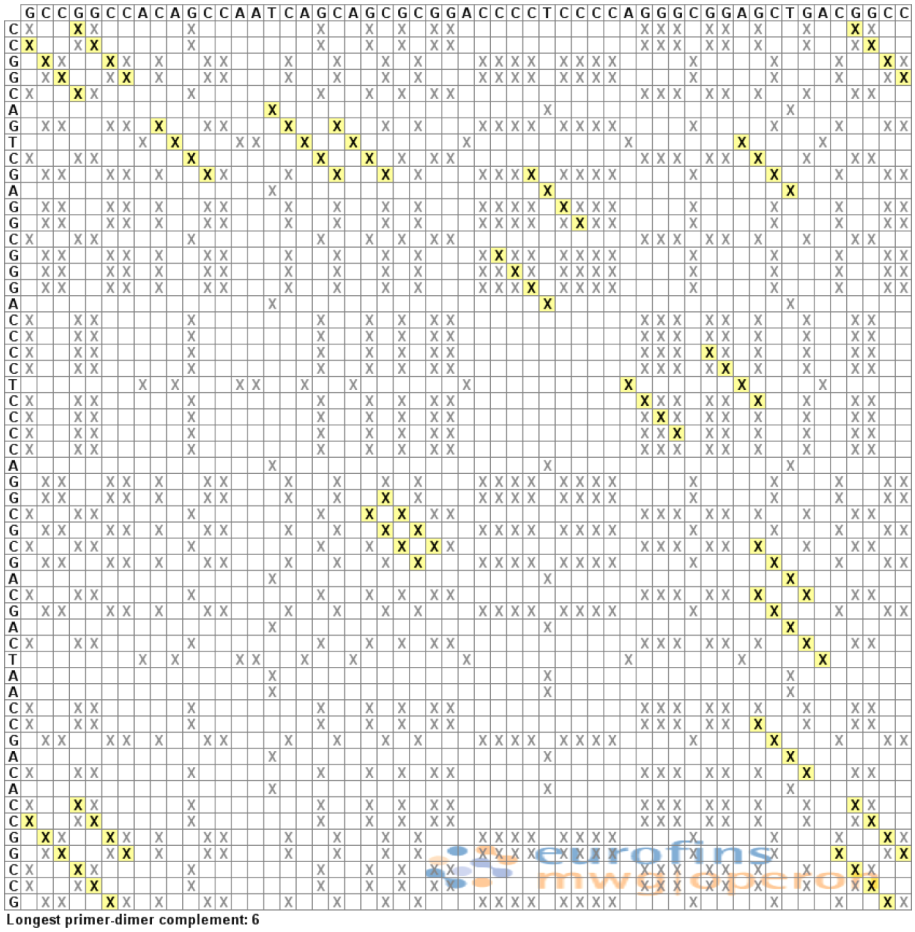

Figure 3. Analysis of complementary sequences in ssDNA. The complementary sequences are marked with yellow "×" sign. The image is generated via the online sequence analysis tool from Operon Inc.

series of AFM topographic images of ssDNA fibers on HDT/Au were acquired at various incubation times (Figure 1). Linear ssDNA fibers with lengths of 20−400 nm could be observed after 5 h incubation time (Figure 1a). The height of the ssDNA fibers is approximately 2.00 ± 0.25 nm. As reported before, the single DNA chain height was about 0.5 nm by TMAFM in air;[16,17] the increased height might be due to the DNA helical structure or some DNA chains that were overlapped in the fiber. After 10 h of incubation, branched fibers appeared (Figure 1b) with a significant height increase (5.50 ± 0.55 nm). The length and the number of fibers were progressively increased (Figure 1c) after 14 h. However, at such long times the height of the ssDNA fibers decreased from 5.50 ± 0.55 to 3.55 ± 0.35 nm. After 22 h of incubation (Figure 1d), it was observed that DNA fibers were densely packed and well organized and the fractal-shaped ssDNA fibers were formed with a significantly increased coverage. These fractal-shaped fibers in one branch neither connect to other branches nor collapse over each other. With the increase of the incubation time, the height of the DNA fibers gradually decreased to 3.45 ± 0.30 nm (22 h) in the end, which is similar to the height observed at an incubation time of 14 h. It indicated that the overlapped bundles in DNA fibers first formed and then dispersed into narrower but longer bundles. After that, the height had no distinguishable change when the incubation time was further increased to 22 h. The height of the fibers was still

dx.doi.org/10.1021/jp306269n | J. Phys. Chem. B 2012, 116, 11594−11599

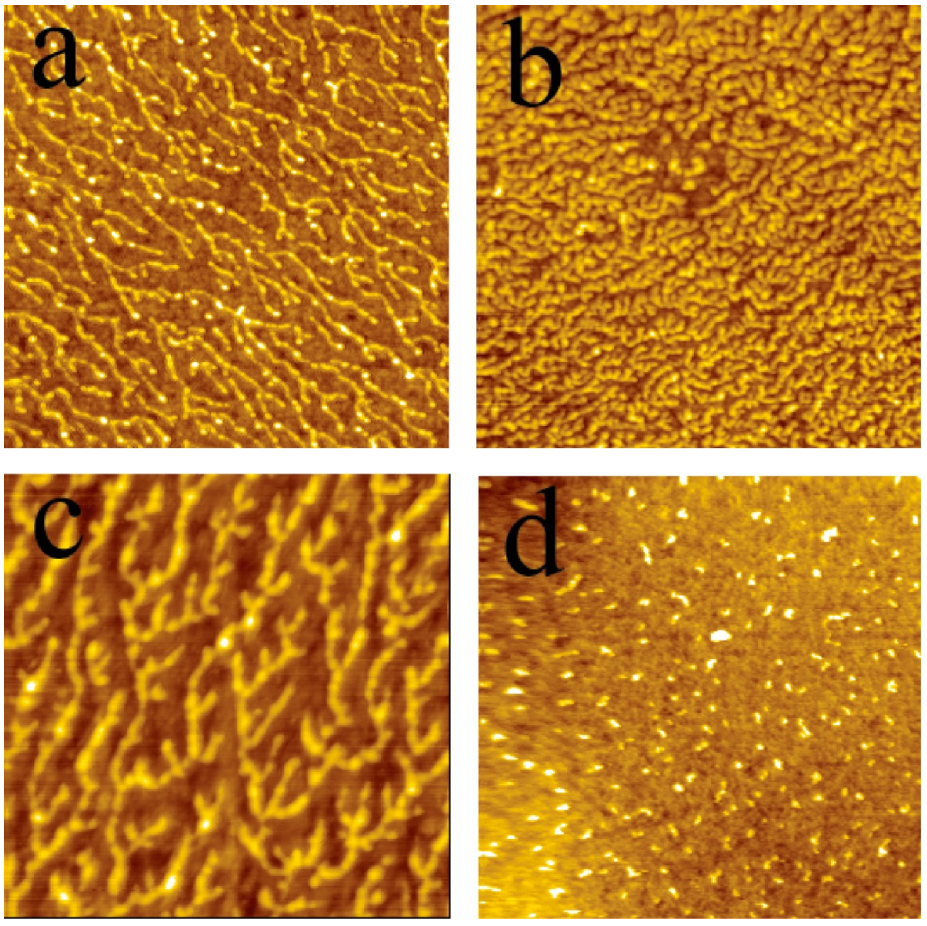

Figure 4. AFM topographic images of the HDT/Au substrate incubated in 1 μmol/L ssDNA (a) probe 2, (b) probe 3, (c) probe 4, and (d) probe 5 for 22 h. The scanning size is 2.0 × 2.0 μm^2.

higher than that of a single DNA chain. This might be due to that some DNA molecules failed to rearrange themselves into separate ones and some sticky ends created by breaking the DNA chains during sample handling that bound other chains to form triple-stranded DNA.[18−20] The heights of the ssDNA fibers for different incubation times were measured from section analysis of the AFM images, and the histogram of different heights was shown in Figure 2a. It was also found that the surface coverage continuously and gradually increased from 7.85 to 62.75% with the increase of the incubation time (Figure 2b). This suggested that the length of ssDNA fibers increased with the incubation time.

Possible Formation Mechanism of DNA Fibers. The binding force between the ssDNA fibers and the SAMs might be hydrogen bonding weak interactions. The nonspecifically adsorbed ssDNA on the HDT SAMs might act as seeds for the subsequent aggregation. During incubation, ssDNA molecule will anchor to the seed ssDNA. When the cooperative process repeated, the whole ssDNA fibers will firmly anchor on the HDT SAMs. The observed diameter is several times that of a single DNA chain.[16,17] By analogy, the 55-mer ssDNA (probe 1) is tens of nanometers long, however, the DNA fibers are thousands of nanometers in length. These indicate that ssDNA fibers must consist of many self-assembled ssDNA molecules.[18−20] In this respect, it is important to note that there was a great deal of complementary regions between two ssDNA (probe 1) sequences (Figure 3), which could lead to base pairing between the two ssDNA (probe 1) molecules. The intermolecular hydrogen bonds between ssDNA molecules might provide the driving forces for the self-assembly of the ssDNA fibers. To verify this hypothesis, the ssDNA fibers were incubated in water at 55 °C for 10 h, whereupon no fibers could be found on the HDT SAM. This observation could be nicely explained by the expected dissociation of the negatively charged DNA double strands at zero ionic strength and elevated temperature.[12]

To prove our hypothesis, control experiments were performed with other four ssDNA. Figure 4 showed AFM topographic images of the HDT/Au substrate after being incubated in 1 μmol/L ssDNA (probe 2; Figure 4a), ssDNA (probe 3; Figure 4b), ssDNA (probe 4; Figure 4c), and ssDNA (probe 5; Figure 4d) for 22 h, respectively. Similar to ssDNA (probe 1), ssDNA (probe 2), ssDNA (probe 3), and ssDNA (probe 4) also formed fibers on the HDT/Au substrate. No fiber formation was observed for the ssDNA (probe 5) case. For the single-stranded DNA that formed fibers (probes 1−4), it could be found that there were complementary regions in their sequences for the interstrand base pairing. In contrast, there is no complementary nucleotide on another ssDNA (probe 5), so that ssDNA (probe 5) cannot self-assemble into fibers.

The resulting highly branched structures were similar to the fractal patterns that had been observed in the DLA of colloids.[21] DLA is a classical model which describes matter irreversibly combines to form dust, soot, and dendrites when the rate-limiting step is the diffusion of matter to the

dx.doi.org/10.1021/jp306269n | J. Phys. Chem. B 2012, 116, 11594−11599

aggregate.[22] The fractal dimension can be used as a quantitative measure of the self-similarity of the fractal across length scales, and it also measures the rate of accumulation of structural detail with increasing magnification. Because the fractal dimension revealed the mechanism of the formation of fractals, we used the Image J (NIH, Bethesda, MD, http://rsbweb.nih.gov/ij/) to estimate the fractal dimension of the ssDNA nanostructures from the AFM images. The fractal dimensions were calculated using the box-counting algorithm. The topography images were converted to an 8-bit binary format and box values of 2, 4, 8, 16, 32, 64, and 128 were overlaid on the image as described earlier.[23,24] The slope of the plot of log (size) versus log (count) corresponds to the negative of the fractal dimension (D). Figure 5 was the calculation of the fractal dimension of the

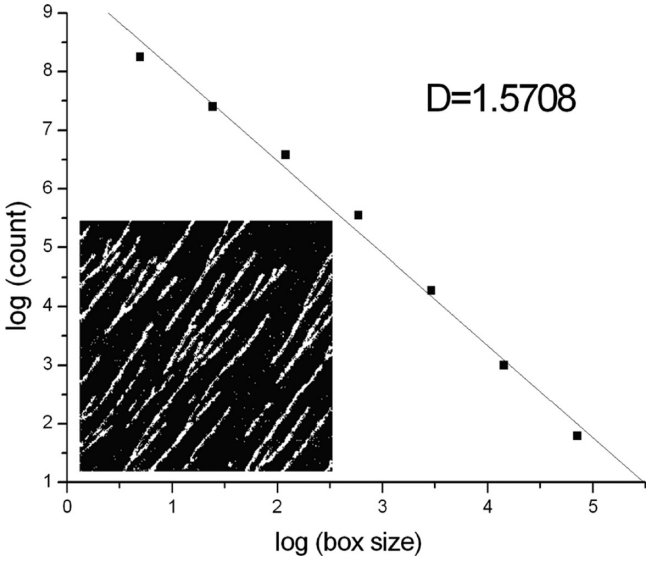

Figure 5. Calculation of the fractal dimension of the ssDNA nanostructure using the box-counting algorithm. The inset shows the image of ssDNA that was used for this calculation (inverted for clarity).

ssDNA (probe 1) nanostructure using the box-counting algorithm. The inset showed the image of ssDNA that was used for this calculation. From this plot, the dimension of the ssDNA fibers fractal was calculated to be 1.5708. The other fractal dimension values of all the patterns in AFM images were listed in Table 1.

The mechanism of the ssDNA fibers formation can be explained by the diffusion-limited aggregation (DLA) theory.[21] The observed ssDNA fibers were quite similar to the DLA generated fractal shape by experiments and simulations.[25−27] Nonspecifically adsorbed ssDNA on the HDT SAM might act as a seed for the subsequent DLA process. During incubation, another ssDNA will either escape to infinity or irreversibly stick to the seed to become a dimer. When the third ssDNA sticks to the dimer, the DNA dimer will become a trimer. As the process was repeated, the assembly grew longer, leading to a fractal shape.

Effect of Terminal Groups of SAMs on Forming Fractal-Shaped ssDNA Fibers. To investigate the effect of terminal groups of SAMs on forming fractal-shaped ssDNA fibers, mercaptans with different terminal groups were explored. Figure 6 is a series of typical AFM topographic images of ssDNA incubated in 1 μmol/L ssDNA (probe 1) for 22 h on SAMs with different terminal groups. ssDNA fibers could not form on the SAMs of 16-mercaptohexadecanoic acid (MHA; Figure 6a), 4-aminothiophenol (4-ATP; Figure 6b), and 6-mercapto-1-hexanol (MCH; Figure 6c). The ssDNA scattered on the SAM of MHA, 4-ATP and MCH, and there were some clusters on the surface. The images show small, isolated objects of uniform size. The smallest objects are most likely individual ssDNA molecules and have a round shape of 20−25 nm diameter, determined as the full width at half-maximum (fwhm) of topography cross sections; the corresponding heights are about 1.0 ± 0.1 nm. In contrast to the SAMs of MHA, 4-ATP, and MCH, ssDNA fibers could form densely on the SAMs of DDT (Figure 6d) and HDT (Figure 1). The terminal groups of DDT and HDT are alkyl while the terminal groups of MHA, 4-ATP, and MCH are carboxyl, amino, and hydroxyl, respectively. Therefore, it implies that fractal-shaped ssDNA fibers may prefer to form on hydrophobic SAMs instead of hydrophilic SAMs.

CONCLUSION

This study described the first observation of ssDNA self-assembly into fractal fibers on an ultraflat gold covered with a SAM of HDT. The duration of incubation time provided for convenient control over different morphologies, such as globes, lines, and nanofibrils. The nanoscale characterization and imaging of the branched patterns formed by the self-assembly of ssDNA were observed via high resolution AFM imaging. The DNA fibers could only form on hydrophobic SAMs and the ssDNA had to have complementary regions in their sequences. This two-dimensional assembly approach generated long DNA fibers with fractal dimensions in the range of 1.49 to 1.93. The method described here should be useful, not only for the construction of fractal patterns, but also for enriching the mechanistic knowledge about the self-assembly of DNA. Importantly, by proper adjustment of the incubation time, different fractal structures can be controlled and immobilized on the surface, which may provide an ideal template for potential technological applications. It may be possible to engineer the fractal nature of ssDNA self-assembly and to direct its assembly to form nanofibrils based on these architectures. This opens up exciting possibilities for the design and fabrication of functional DNA-based, self-assembled materials that exhibit self-similarity at multiple length scales.

Table 1. Fractal Dimension Values of All the Patterns in AFM Image

	HDT/Au (Figure 1, probe 1)							
	Figure 1a (5 h)	Figure 1b (10 h)	Figure 1c (14 h)	Figure 1d (22 h)	HDT/Au (Figure 4a, probe 2)	HDT/Au (Figure 4b, probe 3)	HDT/Au (Figure 4c, probe 4)	DDT/Au (Figure 6d, probe 1)
dimension	1.4993	1.5708	1.8102	1.8791	1.8439	1.9253	1.7933	1.8626

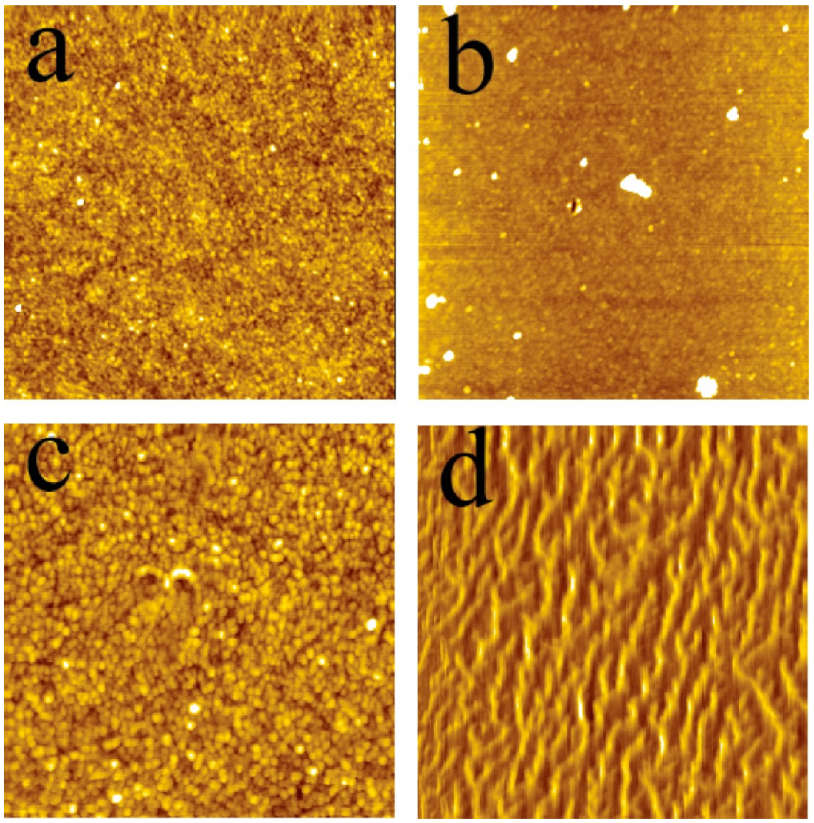

Figure 6. AFM topographic images of ssDNA (probe 1) on (a) MHA/Au, (b) 4-ATP/Au, (c) MCH/Au, and (d) DDT/Au incubated in 1 μmol/L ssDNA for 22 h. The scanning size is 2.0 × 2.0 μm^2.

AUTHOR INFORMATION

Corresponding Author

*Tel./Fax: +86 431 85262430 (B.Z.); +86 431 85262734 (J.T.). E-mail: blzhang@ciac.jl.cn; jltang@ciac.jl.cn.

Notes

The authors declare no competing financial interest.

ACKNOWLEDGMENTS

This work was supported by the National Basic Research Program of China (No.2011CB935800), the National Science Foundation of China (Nos. 20735001, 20975096), and Program of Knowledge Innovation, Chinese Academy of Sciences (KJCX2-YW-H11).

REFERENCES

(1) Zhang, S. G. *Nat. Biotechnol.* **2003**, *21*, 1171−1178.
(2) Huang, J.; Foo, C. W. P.; Kaplan, D. L. *Polym. Rev.* **2007**, *47*, 29−62.
(3) Adamcik, J.; Jung, J. M.; Flakowski, J.; De Los Rios, P.; Dietler, G.; Mezzenga, R. *Nat. Nanotechnol.* **2010**, *5*, 423−428.
(4) Khire, T. S.; Kundu, J.; Kundu, S. C.; Yadavalli, V. K. *Soft Matter* **2010**, *6*, 2066−2071.
(5) Leroux, F.; Gysemans, M.; Bals, S.; Batenburg, K. J.; Snauwaert, J.; Verbiest, T.; Van Haesendonck, C.; Van Tendeloo, G. *Adv. Mater.* **2010**, *22*, 2193−+.
(6) Kyle, S.; Aggeli, A.; Ingham, E.; McPherson, M. J. *Trends Biotechnol.* **2009**, *27*, 423−433.
(7) Lin, M. Y.; Lindsay, H. M.; Weitz, D. A.; Ball, R. C.; Klein, R.; Meakin, P. *Phys. Rev. A* **1990**, *41*, 2005−2020.
(8) Sander, L. M.; Ramanlal, P.; Benjacob, E. *Phys. Rev. A* **1985**, *32*, 3160−3163.
(9) Kurland, N. E.; Kundu, J.; Pal, S.; Kundu, S. C.; Yadavalli, V. K. *Soft Matter* **2012**, *8*, 4952−4959.
(10) Corma, A. *Chem. Rev.* **1997**, *97*, 2373−2419.
(11) On, D. T.; Joshi, P. N.; Kaliaguine, S. *J. Phys. Chem.* **1996**, *100*, 6743−6748.
(12) Gao, P.; Cai, Y. G. *ACS Nano* **2009**, *3*, 3475−3484.
(13) Abramson, G.; Cerdeira, H. A.; Bruschi, C. *BioSystems* **1999**, *49*, 63−70.
(14) Maier, B.; Radler, J. O. *Phys. Rev. Lett.* **1999**, *82*, 1911−1914.
(15) Ercolini, E.; Valle, F.; Adamcik, J.; Witz, G.; Metzler, R.; De Los Rios, P.; Roca, J.; Dietler, G. *Phys. Rev. Lett.* **2007**, *98*, 058102.
(16) Thundat, T.; Allison, D. P.; Warmack, R. J. *Nucleic Acids Res.* **1994**, *22*, 4224−4228.
(17) Lyubchenko, Y. L.; Shlyakhtenko, L. S. *Proc. Natl. Acad. Sci. U.S.A.* **1997**, *94*, 496−501.
(18) Revet, B.; Fourcade, A. *Nucleic Acids Res.* **1998**, *26*, 2092−2097.
(19) Cohen, S. N.; Chang, A. C. Y.; Boyer, H. W.; Helling, R. B. *Proc. Natl. Acad. Sci. U.S.A.* **1973**, *70*, 3240−3244.
(20) Song, Y. H.; Li, Z.; Liu, Z. G.; Wei, G.; Wang, L.; Sun, L. L.; Guo, C. L.; Sun, Y. J.; Yang, T. *J. Phys. Chem. B* **2006**, *110*, 10792−10798.
(21) Witten, T. A.; Sander, L. M. *Phys. Rev. Lett.* **1981**, *47*, 1400−1403.
(22) Jin, Y. D.; Dong, S. J. *Angew. Chem., Int. Ed.* **2002**, *41*, 1040−+.
(23) Murr, M. M.; Morse, D. E. *Proc. Natl. Acad. Sci. U.S.A.* **2005**, *102*, 11657−11662.
(24) Smith, T. G.; Lange, G. D.; Marks, W. B. *J. Neurosci. Methods* **1996**, *69*, 123−136.
(25) Hurd, A. J.; Schaefer, D. W. *Phys. Rev. Lett.* **1985**, *54*, 1043−1046.
(26) Xiao, L. H.; Zhou, R.; He, Y.; Li, Y. J.; Yeung, E. S. *J. Phys. Chem. C* **2009**, *113*, 1209−1216.
(27) Roder, H.; Hahn, E.; Brune, H.; Bucher, J. P.; Kern, K. *Nature* **1993**, *366*, 141−143.